



ANNUAL  
REVIEWS **Further**

Click [here](#) to view this article's online features:

- Download figures as PPT slides
- Navigate linked references
- Download citations
- Explore related articles
- Search keywords

# Water-Mediated Hydrophobic Interactions

Dor Ben-Amotz

Department of Chemistry, Purdue University, West Lafayette, Indiana 47907;  
email: [bendor@purdue.edu](mailto:bendor@purdue.edu)

Annu. Rev. Phys. Chem. 2016. 67:617–38

The *Annual Review of Physical Chemistry* is online at [physchem.annualreviews.org](http://physchem.annualreviews.org)

This article's doi:

10.1146/annurev-physchem-040215-112412

Copyright © 2016 by Annual Reviews.

All rights reserved

## Keywords

hydrophobic, water-mediated, potential of mean force, free energy, enthalpy, entropy, compensation, crossover

## Abstract

Hydrophobic interactions are driven by the combined influence of the direct attraction between oily solutes and an additional water-mediated interaction whose magnitude (and sign) depends sensitively on both solute size and attraction. The resulting delicate balance can lead to a slightly repulsive water-mediated interaction that drives oily molecules apart rather than pushing them together and thus opposes their direct (van der Waals) attraction for each other. As a consequence, competing solute size-dependent crossovers weaken hydrophobic interactions sufficiently that they are only expected to significantly exceed random thermal energy fluctuations for processes that bury more than  $\sim 1 \text{ nm}^2$  of water-exposed area.

## 1. INTRODUCTION

Although we are accustomed to thinking of oil-water interactions as “phobic,” the substantial attraction of water to oil plays a key role in tipping the delicate hydrophobic balance just enough to render nonpolar molecules useful for the self-assembly of living systems and bioinspired devices. Describing this emerging understanding (1, 2), with its subtle nuances and surprising twists, is the primary aim of this review. This is a story about what makes water unique as a solvent—highlighting the role of oil-water attraction in both increasing solubility and damping hydrophobic interactions—to facilitate the emergence of dynamically responsive structures that live at the precipice of instability. Be forewarned that, while a satisfyingly cohesive picture of hydrophobicity is emerging, one may find parts of this story to be both disturbing and provocative, as it upends common misconceptions regarding hydrophobicity and highlights open questions pertaining to the role of crossover length scales and cooperativity in driving hydrophobic self-assembly.

Water-mediated hydrophobic interactions are intimately linked to hydrophobic hydration, as the former arise from the latter. In other words, the water-mediated interaction free energy of a hydrophobic aggregate is precisely equal to the difference between its hydration free energy and the sum of the hydration energies of the individual (nonaggregated) molecules. Stated in yet another way, the total interaction free energy of a pair of solutes in water is equivalent to their potential of mean force  $w(\tau) = u(\tau) + \Delta w(\tau)$ , where  $u(\tau)$  is the direct interaction energy of the solutes (in absence of water), and  $\Delta w(\tau) = w(\tau) - u(\tau)$  is the water-mediated contribution to  $w(\tau)$ . For spherical solutes, the variable  $\tau$  is simply equal to the distance between their centers, while for solutes of more general structure  $\tau$  represents a collection of variables that define the relative separation, orientation, and internal configurations of the two solute molecules. More generally still,  $w(\tau)$  may represent the interaction free energy of a collection of multiple solutes, where  $u(\tau)$  and  $\Delta w(\tau)$  are again the corresponding direct and water-mediated contributions to  $w(\tau)$ . Both the magnitude and sign of  $\Delta w(\tau)$  depend remarkably sensitively on oil-water attractive interactions. Moreover, the attraction between water and aliphatic groups places them very close to the boundary between hydrophobic and hydrophilic regimes. Thus, whereas the hydration thermodynamics of oily molecules are characteristically hydrophobic, their water-mediated interactions can be hydrophilic, as water may pull oily molecules apart rather than pushing them together.

This delicate hydrophobic balancing act, which arises from the near-perfect cancellation of large repulsive and attractive contributions, is one of the many unique features of water as solvent (3–6). This cancellation sets water apart from other solvents—situating water near no solvent at all—as the interactions between oily molecules in water are substantially dictated by their direct interactions with each other (as in the gas phase). This behavior stands in marked contrast to nonaqueous solvents, in which the conformations and interactions of oily molecules differ greatly from the gas phase. Thus, the term hydrophobicity is most appropriate in distinguishing the solvation of oily molecules in water and organic solvents, whereas, with respect to the gas phase, oily molecules are not so very hydrophobic after all.

This review is focused rather narrowly on hydrophobic hydration and interaction thermodynamics, with particular emphasis on the interplay of repulsive (entropic) and attractive (energetic) interactions between water and oily molecules. Additional background may be found in previous influential discussions of hydrophobicity (7–18). Blokzijl & Engberts’ (19) 1993 review provides a uniquely valuable compilation of early experimental results. Chandler’s (20) 2005 *Nature* Insight review presents a lucid exposition of the relevance of length scales to hydrophobic phenomena, building on prior work (21, 22) and ideas insightfully described by Hummer and coworkers (23), although a key water-mediated interaction approximation invoked in the latter discussion has since been updated (24). Pettitt and coworkers (24a–24c) have recently highlighted open questions

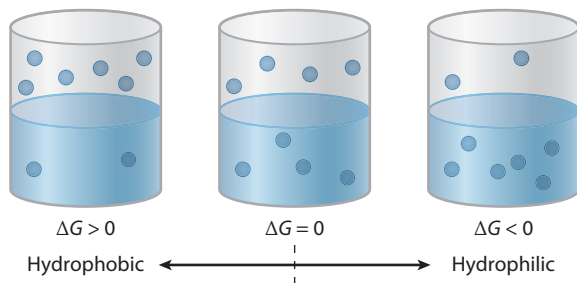


**Figure 1**

A solute's solvation free energy reflects its equilibrium concentration ratio in the gas and liquid phase. Figure adapted from Reference 37 with permission. Copyright 2008 American Chemical Society.

regarding the influence of solute shape on hydrophobicity. The central role of hydrophobicity in host-guest binding (25–30) is eloquently reviewed by Hillyer & Gibb (31) in their companion article in this volume. Readers particularly interested in the biological role of water and hydrophobicity should be aware of valuable previous reviews (5, 28, 32, 33). Some of the latter issues are discussed in Section 4, after a review of the thermodynamics of hydrophobic hydration and interactions in Sections 2 and 3.

## 2. HYDROPHOBIC HYDRATION THERMODYNAMICS

### 2.1. Ben-Naim Solvation Process

All the solvation thermodynamic quantities described in this work pertain to a Ben-Naim solvation process, corresponding to the transfer of an isolated (gas-phase) stationary solute into water, as further described by Ben-Naim (34, 35) (and in the **Supplemental Appendix**; follow the **Supplemental Material link** from the Annual Reviews home page at <http://www.annualreviews.org>). The associated partial molar solvation free energy  $\Delta G$  is directly related to the Ostwald absorption coefficient  $\rho_L/\rho_V$ , where  $\rho_L$  and  $\rho_V$  are the equilibrium number densities (or concentrations) of the solute in the liquid ( $L$ ) and gas ( $V$ ) phase:

$$\Delta G = G(L) - G(V) = -RT \ln \left( \frac{\rho_L}{\rho_V} \right). \quad (1)$$

Thus,  $\Delta G = 0$  implies that the equilibrium concentrations of the solute are the same in the vapor and liquid phases, whereas  $\Delta G > 0$  implies that the equilibrium concentration of the solute in the liquid is smaller than that in the gas (and conversely when  $\Delta G < 0$ ), as illustrated in **Figure 1**.

### 2.2. Influence of Solute-Solvent and Solvent-Solvent Interactions

The combined experimental and molecular dynamics (MD) simulation results (36–41) shown in **Figure 2** reveal that all alkanes have remarkably similar positive, and relatively small, hydration free energies arising from a nearly perfect cancelation of the attractive ( $E_{UV}$ ) and repulsive ( $-TS_{UV}$ ) solute-solvent ( $UV$ ) interactions (as further explained below). By contrast, the self-solvation free energies of  $n$ -alkanes (in oil, **Figure 2a**) are negative and approximately linearly correlated with  $n$ -alkane chain length. Moreover, MD simulations of  $n$ -alkanes (up to  $n$ -C<sub>22</sub>) in water and the gas phase by Ferguson et al. (41) revealed that both the radii of gyration and folding mean force potentials of  $n$ -alkanes are nearly the same in water and the gas phase. Yet, there is little doubt that a long  $n$ -alkane chain, which spontaneously folds upon itself in the gas phase, will spontaneously

Supplemental Material

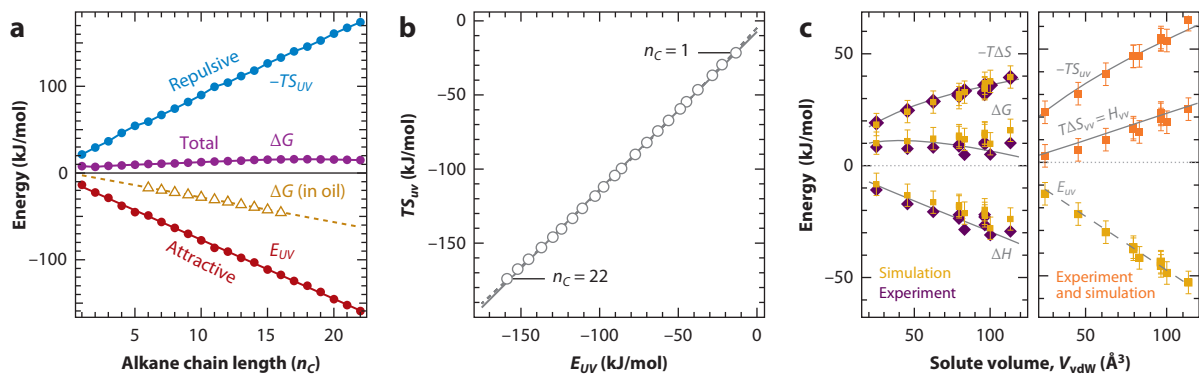


**Figure 2**

(a) The hydration free energy  $\Delta G$  of  $n$ -alkanes from  $\text{CH}_4$  ( $n_c = 1$ ) to  $n\text{-C}_{22}\text{H}_{46}$  ( $n_c = 22$ ) is the sum of nearly equal and opposite contributions from solute-water interaction energy  $E_{UV}$  and fluctuation entropy  $TS_{UV}$  (36). There is good agreement between the  $\Delta G$  values obtained experimentally and using classical (TraPPE/SPC-E) simulations (41). The  $E_{UV}$  values are obtained using classical (OPLS-AA/TIP4P) simulations (36). The triangular (brown) points represent the experimental solvation energies of alkanes in their own pure liquids (49), which, unlike their hydration free energies, scale approximately linearly with chain length ( $\Delta G_{\text{in oil}} \approx 0.429 - 2.84n_c$ ), as do the interaction energies of alkanes with water ( $E_{UV} \approx -8.77 - 6.805n_c$ ). (b) The correlation between  $E_{UV}$  and  $TS_{UV}$  is nearly linear ( $TS_{UV} \approx -7.266 + 1.064E_{UV}$ ) (solid line) but is slightly better represented by a quadratic function ( $TS_{UV} \approx -4.707 + 1.1425E_{UV} + 0.000453E_{UV}^2$ ) (dashed curve) (36). (c, left column) Hydration thermodynamic functions of linear, branched, and cyclic alkanes (with up to six carbons), and (right column) the corresponding solute-solvent and solvent reorganization energies and entropies, plotted as a function of solute van der Waals volume (37). The dark purple points represent experimental measurements (38), the gold points are classical (OPLS-AA/TIP4P) simulation results (39, 40), the orange points are obtained by combining experimental and simulation measurements, and the curves represent linear-response (first-order thermodynamic perturbation theory) predictions (37). Panels a and b adapted from Reference 37 with permission. Copyright 2008 American Chemical Society. Panel c adapted from Reference 36 with permission. Copyright 2010 American Chemical Society.

unfold when transferred to a nonpolar solvent, driven by the favorable entropy of unfolding and the absence of a significant enthalpic penalty to unfolding in a nonpolar solvent. This suggests that, as far as oily solutes are concerned, water more closely resembles a gas (no solvent at all) than it does an organic solvent.

**Figure 2c** shows how the experimental hydration thermodynamic functions ( $\Delta G$ ,  $\Delta H$ , and  $T\Delta S$ ) of various linear and branched alkanes are related to the underlying solute-solvent ( $UV$ ) and solvent-solvent ( $VV$ ) interaction energies and entropies. The most important point is that  $\Delta G = E_{UV} - TS_{UV}$  is determined entirely by direct solute-solvent interactions, whereas  $\Delta H$  and  $\Delta S$  contain additional contributions due to solute-induced changes in solvent-solvent interactions that must necessarily exactly compensate  $\Delta H_{VV} = T\Delta S_{VV}$  and so do not directly contribute to  $\Delta G$  (43). Moreover, **Figure 2b** indicates that  $E_{UV}$  and  $TS_{UV}$  are also highly correlated and approximately equal to each other (36). The following more detailed discussion of these issues may be of most interest to aficionados of statistical mechanics. Other readers would do themselves no harm by leaping directly from here to Section 2.3.

The Widom potential distribution theorem (in its inverse form) (42) yields the following exact theoretical expressions for  $\Delta G$  (37, 43, 44), although Equation 2 was first derived in other ways (45, 46):

$$\Delta G = RT \ln \langle e^{\Psi/RT} \rangle = \langle \Psi \rangle + RT \ln \langle e^{\delta\Psi/RT} \rangle \equiv E_{UV} - TS_{UV}. \quad (2)$$

The variable  $\Psi$  represents the direct interaction energy between the solute and all the solvent molecules (in a particular solvent conformation) and the angle brackets indicate an average over all equilibrium configurations of the solution (at a constant temperature and volume, such that the

average pressure of the system is equal to the experimental pressure of interest). Thus,  $\langle \Psi \rangle = E_{UV}$  is the average solute-solvent interaction energy. More specifically,  $\Psi$  represents the difference between the total energy of the system with and without the solute present (in a particular, fixed, solvent configuration), and thus the definition of  $\Psi$  does not require assuming that intermolecular interactions are two-body additive (43). However, in a system with two-body additive interactions,  $\Psi$  is equivalent to the sum of the two-body interaction energies of the solute and all the surrounding solvent molecules.

The energy difference  $\delta\Psi = \Psi - \langle \Psi \rangle$  represents the fluctuations in  $\Psi$  relative to its average value, and thus  $\sigma = \sqrt{\langle \delta\Psi^2 \rangle}$  is the standard deviation of  $\delta\Psi$ . Equation 2 identifies  $-TS_{UV} = RT \ln\langle e^{\beta\delta\Psi} \rangle \approx \frac{1}{2}\beta\sigma^2 > 0$  (where  $\beta = 1/RT$ ) as the entropic contribution to  $\Delta G$  arising from fluctuations in the direct interaction energy between the solute and solvent. Note that  $\frac{1}{2}\beta\sigma^2$  would be exactly equal to  $-TS_{UV}$  if the energy fluctuations were strictly Gaussian (which would in turn imply that solute-solvent interactions may be described by linear response theory or equivalently by second-order thermodynamic perturbation theory) (37, 43, 47, 48). Moreover,  $S_{UV}$  is invariably negative and increases with increasing  $\sigma^2 = \langle \delta\Psi^2 \rangle$ .

The direct solute-solvent interaction energy  $E_{UV}$  is not equivalent to either the solute's hydration energy  $\Delta U$  or enthalpy  $\Delta H$ , as the latter quantities contain an additional water-reorganization energy,  $\Delta U_{VV} = \Delta H_{VV} - PV$ , arising from the change in the water-water interaction energy induced by the solute (of partial molar volume  $V$ ) (36, 43). However, this water-reorganization enthalpy does not contribute directly to  $\Delta G$  because it is exactly cancelled (compensated) by the corresponding water reorganization entropy,  $T\Delta S_{VV} = \Delta H_{VV}$ , and thus  $\Delta H_{VV} - T\Delta S_{VV} = 0$ , as required by Equation 2, because  $\Delta G = \Delta H - T\Delta S = E_{UV} - TS_{UV}$ :

$$\Delta H = E_{UV} + \Delta U_{VV} + PV = E_{UV} + \Delta H_{VV}, \quad (3)$$

$$T\Delta S = TS_{UV} + T\Delta S_{VV} = TS_{UV} + \Delta H_{VV}. \quad (4)$$

Although Equation 2 indicates that the solvent reorganization energy and entropy do not directly influence  $\Delta G$ , they can indirectly do so because  $E_{UV}$  and  $S_{UV}$  depend on the structure of the water molecules surrounding the solute and that structure also determines  $T\Delta S_{VV} = \Delta H_{VV}$ . Moreover,  $\Delta S = -(\partial\Delta G/\partial T)_P$ , so solvent reorganization does contribute to the temperature dependence of  $\Delta G$ .

### 2.3. The Influence of Temperature

**Figure 3** compares the hydration thermodynamics of xenon (Xe) and methane (CH<sub>4</sub>) (38) with the self-solvation thermodynamics of *n*-hexane in its own pure liquid (49) over an exceptionally wide temperature range (along the vapor-liquid coexistence curve) obtained from experimental data compiled in the ORCHYD (38) and NIST (49) databases (see the **Supplemental Appendix**). A wealth of insights regarding hydrophobic hydration and the unique properties of water as a solvent may be gleaned from these results. For example, the hydration free energies  $\Delta G$  of the nonpolar solutes remain approximately constant (and slightly positive) over an enormous temperature range, whereas the corresponding enthalpies  $\Delta H$  and entropies  $T\Delta S$  are strongly temperature dependent and highly correlated with each other. When  $\Delta H$  crosses zero, the hydration process is entirely entropy dominated (as  $\Delta G = -T\Delta S$ ), whereas when  $\Delta S$  crosses zero, it is entirely enthalpy dominated (as  $\Delta G = \Delta H$ ). The fact that  $\Delta G$  remains approximately constant over this temperature range suggests that there are large compensating contributions to  $\Delta H$  and  $T\Delta S$  that do not directly contribute to  $\Delta G$ —thus questioning the utility of referring to  $\Delta G$  as either enthalpy or entropy “driven.” Although  $\Delta G$  is approximately temperature independent, it cannot

 [Supplemental Material](#)

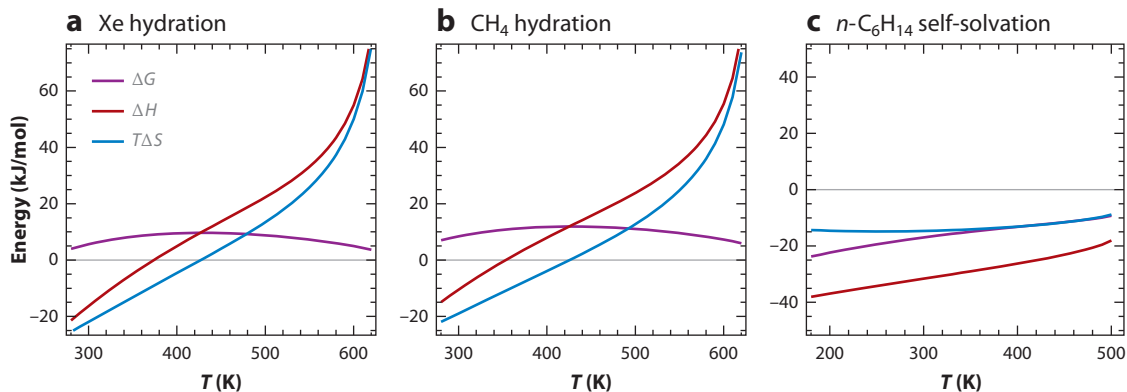


**Figure 3**

Experimental temperature dependence of the hydration thermodynamics of (a) xenon (Xe) and (b) methane (CH<sub>4</sub>) (38); (c) self-solvation of *n*-hexane (*n*-C<sub>6</sub>H<sub>14</sub>) (49).

be precisely constant, as the nonmonotonic temperature dependence of  $\Delta G$  is linked to the fact that  $\Delta S = -(\partial\Delta G/\partial T)_P$ , and thus  $\Delta G$  must attain a maximum when  $\Delta S = 0$ . The nearly linear temperature dependence of  $\Delta H$  (up to  $T \approx 500$  K) implies that the corresponding hydration heat  $\Delta C_P = C_P(L) - C_P(G) = (\partial\Delta H/\partial T)_P$  is large and positive, and roughly constant, except at temperatures approaching the critical point of water ( $T_c \approx 647$  K). The characteristically large temperature derivative of  $\Delta H$  (and  $T\Delta S$ ) for hydrophobic hydration processes (19, 44, 50) contrasts with the self-solvation thermodynamics of *n*-hexane (shown in **Figure 3c**), which is typical of nonaqueous solvation processes.

Paschek's (51, 52) MD studies of the hydration thermodynamics of Xe in water predict that, although  $\Delta H_{VV}$  is strongly temperature dependent,  $E_{UV}$  is not. This implies that  $\Delta C_P = (\partial E_{UV}/\partial T)_P + (\partial\Delta H_{VV}/\partial T)_P$  is largely determined by the temperature dependence of the water reorganization enthalpy  $\Delta H_{VV}$  around a hydrophobic solute (44). Moreover, because both  $E_{UV}$  and  $\Delta G$  are nearly temperature independent, so must  $TS_{UV}$  be. In other words, the temperature independence of  $\Delta G$  can be traced to the fact that the direct interaction energy of Xe with water is determined primarily by the density of liquid water, which is itself remarkably temperature independent (49). By contrast,  $\Delta H$  is substantially influenced by the water-reorganization enthalpy  $\Delta H_{VV}$  and thus is sensitive to solute-induced changes in water H-bonds, which are largely retained at low temperatures but significantly disrupted at high temperatures, consistent with a tenuous clathrate-like structure of the hydration shell surrounding nonpolar solutes (18, 53).

The approximately constant temperature derivative of  $\Delta H$  over the normal liquid temperature range of water (see **Figure 3a,b**) implies that the temperature dependence of  $\Delta G$ ,  $\Delta H$ , and  $\Delta S$  for hydrophobic hydration process may be represented reasonably accurately by treating  $\Delta C_P$  as a temperature-independent constant (43, 44, 54). However, the relatively small variations in the temperature derivative of  $\Delta H$  indicate that  $\Delta C_P$  is not in fact constant, as illustrated in **Figure 4**, which shows the temperature dependence of the hydration heat capacities of Xe, CH<sub>4</sub>, and three alcohols: ethanol (C<sub>2</sub>H<sub>5</sub>OH), *n*-propanol (*n*-C<sub>3</sub>H<sub>7</sub>OH), and *n*-pentanol (*n*-C<sub>5</sub>H<sub>11</sub>OH). Similar results (over a narrower temperature range) have been obtained for other nonpolar solutes (55), alcohols (56), and functional groups (57). However, the solvation heat capacities in nonpolar solvents are much smaller and nearly temperature independent, as exemplified by the self-solvation of *n*-hexane (49) and the solvation of Xe in various organic solvents (58, 59).

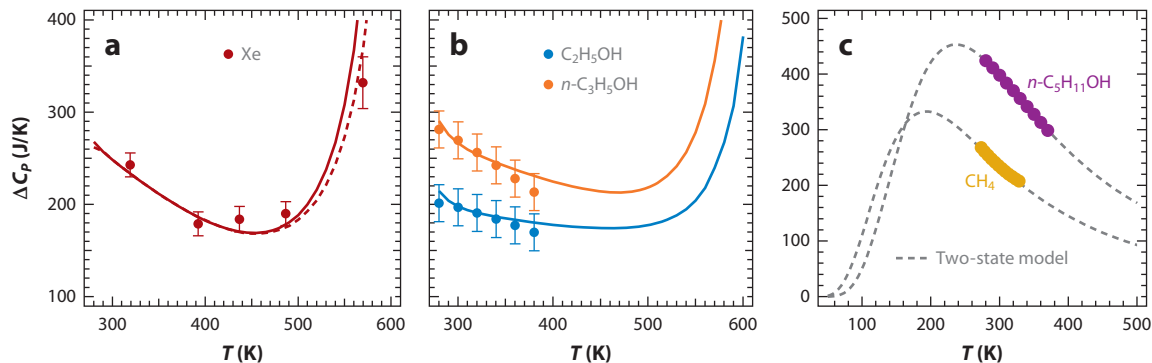


**Figure 4**

Partial molar hydration heat capacities,  $\Delta C_p$ , of (a) xenon, (b) ethanol and *n*-propanol, and (c) methane and *n*-pentanol are plotted as a function of temperature in liquid water (along the vapor-liquid coexistence curve). Solid curves (a,b) are derived from global fits to experimental hydration thermodynamic data (38). Points are (a) directly measured partial molar heat capacities of Xe (62), and (b) obtained from a fit to a large number of experimental measurements performed over the indicated temperature range (56). Dashed curves are (c) obtained from a two-state model fit (63) and (a)  $(\partial\Delta H/\partial T)_{cc}$  obtained from hydration enthalpy of Xe along the water vapor-liquid coexistence curve (38), thus showing that  $(\partial\Delta H/\partial T)_{cc} \approx (\partial\Delta H/\partial T)_p$ , over the normal liquid range of water (see the **Supplemental Appendix**).

[▶ Supplemental Material](#)

The nonmonotonic temperature dependence of hydrophobic heat capacities mirrors the heat capacity of pure water, which also has a minimum in the normal liquid range and increases dramatically at both very low (supercooled) and very high (near critical) temperatures (60). However, unlike the hydration heat capacities of nonpolar solutes, the self-solvation  $\Delta C_p$  of pure water remains remarkably constant over its normal liquid temperature range ( $273 \text{ K} \leq T \leq 373 \text{ K}$ ) and is much smaller,  $\Delta C_p \approx 42 \text{ J/(K mol)}$  (49), than typical hydrophobic  $\Delta C_p$  values (as shown in **Figure 4**).

The increase in  $\Delta C_p$  at high temperatures (as shown in **Figure 4a,b**) is consistent with Wheeler’s lattice model predictions, pertaining to any system in which the solute-solvent interaction energy is less favorable than (or comparable to) the solvent-solvent interaction energy (61, 62). Frank & Evans (18) first recognized the decrease in hydrophobic hydration heat capacities with temperatures in the normal liquid range of water (as exemplified by the results in **Figure 4**). Gill and coworkers (63) have shown that a two-state model of water can approximately reproduce the temperature dependence of  $\Delta C_p$  under this temperature range, as illustrated in **Figure 4c** (see the **Supplemental Appendix**).

Other evidence of two-state behavior has been found in hydrophobic hydration thermodynamics (13, 50, 64, 65) as well as in pure supercooled liquid (66–69) and glassy (70, 71) water. Moreover, simulations have uncovered two structural motifs in the hydrophobic hydration shells of proteins (65, 72), small molecules (10, 65), and nanoparticles (73). The two water structures have variously been described as “clathrate-like” and “inverted” (72) or as consisting of “ice-like” and “bent” H-bonds (10). These structures may be related to the experimentally observed transformation from a more tetrahedral to a more disordered water structure in the hydration shells of *n*-alcohols, with a transition temperature that decreases with increasing aliphatic chain length (53). However, the fact that water often seems to display two-state behavior need not be inconsistent with the presence of a continuum of H-bond strengths, lengths, and angles, as shown by Geissler and coworkers (74, 75).

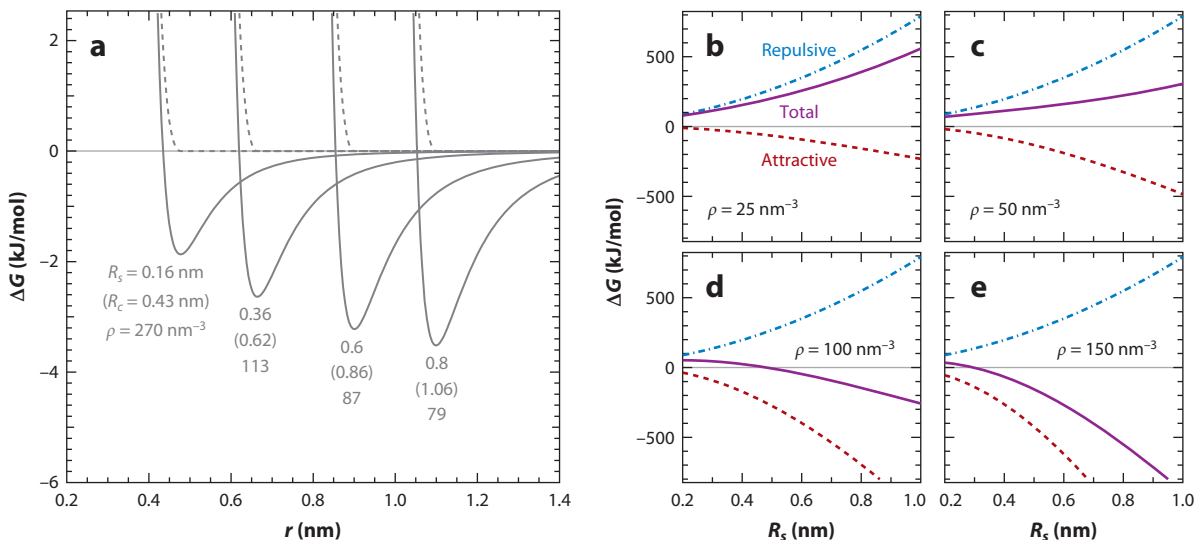


**Figure 5**

(a) Oil-drop potential energies (solid curves) plotted as a function of the distance between the center of the oil drop and the center of a water oxygen atom (76). The oil-drop cavity radius  $R_c$  corresponds to the oil-water separation at which the oil drop's Week-Chandler-Andersen repulsive core potential (dashed curve) is equal to  $RT \approx 2.4$  kJ/mol (77). The hydration thermodynamics of the first and second oil drops are similar to  $n$ -alkanes with 8 and 22 carbons, respectively, and the largest two oil drops have hydration free energies of  $\sim 10$  kJ/mol. (b-e) Total hydration free energy  $\Delta G$  (solid purple curves) for oil drops with various values of  $\rho$  and  $R_s$  plotted along with the corresponding repulsive  $-TS_{UV}$  (cavity formation) (blue dot-dashed curves) and attractive  $E_{UV}$  (oil-water cohesion) (red dashed curves) contributions to  $\Delta G$ , obtained using classical (OPLS-UA/TIP4P) simulations (48). Oil drops with a methyl group density of  $\rho = 100$  nm $^{-3}$  are predicted to cross over from being hydrophobic ( $\Delta G > 0$ ) to hydrophilic ( $\Delta G < 0$ ) at  $R_s \approx 0.48$  nm (which corresponds to a cavity radius of  $R_c \approx 0.74$  nm).

## 2.4. The Influence of Solute Size and Attractive Interactions

The influence of solute size and attractive interactions on hydrophobic hydration thermodynamics may best be illustrated by considering the hydration of model spherical oil drops whose interaction potential with water is obtained by uniformly distributing methyl groups of number density  $\rho$  over a sphere of radius  $R_s$  (76). Note that the radius  $R_s$  that contains the methyl group centers is smaller than the cavity radius  $R_c$  from which the centers of water molecules are excluded (as illustrated in **Figure 5a**; also see the **Supplemental Appendix**).

The hydration thermodynamics of such oil drops may be obtained from a two-step process: First, a purely repulsive sphere (empty cavity) is created in water, and then attractive oil-water interactions are introduced by filling the sphere with a uniform distribution of methyl groups of density  $\rho$  to obtain results such as those shown in **Figure 5b** (48) (also see the **Supplemental Appendix**). Note that the oil-drop hydration free energies  $\Delta G$  are positive (hydrophobic) when  $\rho$  is small and become negative (hydrophilic) when  $\rho$  is large, while at intermediate  $\rho$  values  $\Delta G$  crosses over from the hydrophobic ( $\Delta G > 0$ ) to hydrophilic ( $\Delta G < 0$ ) regime with increasing  $R_s$  (see **Figure 5d,e**).

**Figure 6** shows a global contour plot of the oil-drop hydration free energies as a function of oil-drop size  $R_s$  and methyl group density  $\rho$  to reveal the hydrophobic and hydrophilic domains. The points in **Figure 6** represent the experimental hydration free energies of alkanes whose effective  $R_s$  and  $\rho$  values are self-consistently matched to oil-drop predictions (36, 41). The fact that these points track the  $\Delta G = 0$  curve, makes it clear, once again, that the hydration free energies of

Supplemental Material

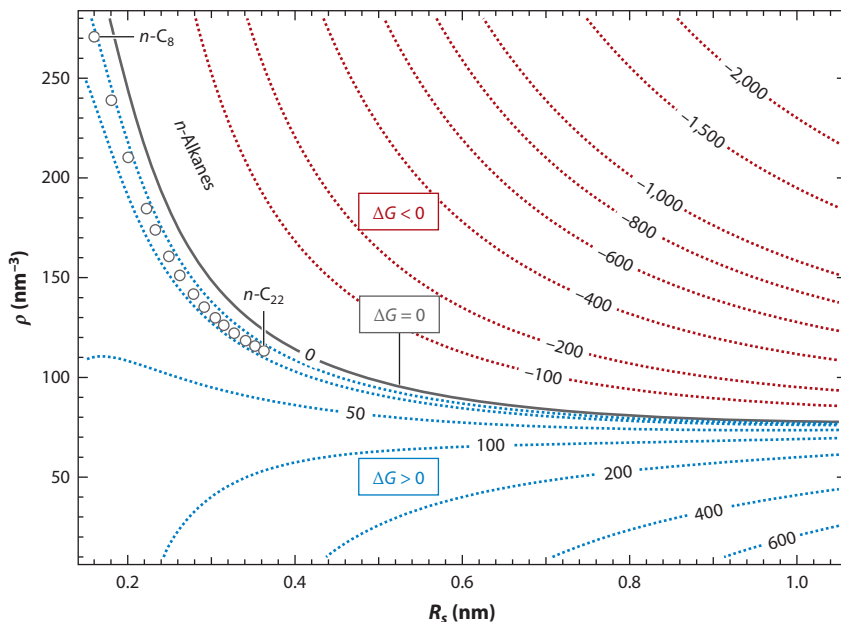


**Figure 6**

Oil-drop hydration free energies  $\Delta G$ , obtained using classical (OPLS-UA/TIP4P) simulations (48), depend on both the radius ( $R_s$ ) and the methyl group density ( $\rho$ ) of the oil drop. Numbers on the contour lines are  $\Delta G$  values in kJ/mol units. The sign of  $\Delta G$  indicates whether the oil drop is hydrophobic ( $\Delta G > 0$ ) or hydrophilic ( $\Delta G < 0$ ). Points represent oil drops whose hydration thermodynamics are similar to those of  $n$ -alkanes with 8–22 carbons (36, 41). The two contours on either side of the  $n$ -alkane points pertain to  $\Delta G = 10$  and 20 kJ/mol. Longer chain  $n$ -alkanes are predicted to have  $\Delta G$  values of similar magnitude, and extrapolations to longer chain lengths imply that  $\Delta G = 0$  at an alkane chain length of approximately  $n$ -C<sub>100</sub> (corresponding to  $R_s \approx 0.9 \pm 0.1$  nm) (36).

alkane molecules reside very near the hydrophobic-hydrophilic boundary (as also evidenced by the results in **Figure 2**). In the next section, we discuss how the underlying delicate balance of repulsive ( $-TS_{UV}$ ) and attractive ( $E_{UV}$ ) oil-water interactions profoundly influences the water-mediated interactions between oily molecules.

The above oil-drop hydration free energy results were obtained assuming that repulsive and attractive hydration free energies are decoupled, as is the case for small oily molecules and oil drops (14, 23, 37, 54). However, for large oil drops, a relatively small amount of free energy coupling is expected to result from the influence of oil-water attractive interactions on hydration-shell water structure (48, 78). This and other approximations employed in calculating  $TS_{UV}$  and  $E_{UV}$  are not expected to significantly alter the oil-drop hydration free energy predictions shown in **Figures 5, 6, and 8** (also see the **Supplemental Appendix**).

 Supplemental Material

### 3. WATER-MEDIATED HYDROPHOBIC INTERACTIONS

#### 3.1. Overview of Theoretical and Experimental Results

Purely repulsive (hard-sphere) solutes, approximately the size of CH<sub>4</sub>, are driven to aggregate by a water-mediated (entropic depletion) interaction with a contact free energy of  $w(r_c) = \Delta w(r_c) \approx -4$  kJ/mol (24). However, two CH<sub>4</sub> molecules dissolved in water are predicted to have a shallower

contact free energy of  $w(r_c) \approx -2.5$  kJ/mol, over half of which is due to the direct attraction between  $\text{CH}_4$  molecules, and so  $\Delta w(r_c) \approx -1$  kJ/mol for  $\text{CH}_4$  in water (1). Thus, methane-water attraction is evidently responsible for the substantial decrease in  $\Delta w(r_c)$  (by a factor of  $\sim 4$ ). These results imply that oil-water attraction decreases  $\Delta w$ , as it stabilizes the hydration shell around each oil molecule and thus disfavors direct oil-oil contacts. However, accurately predicting  $w(r)$  and  $\Delta w(r)$  remains a significant challenge, as attested by disparities between mean force potential predictions obtained using various classical and quantum mechanical modeling strategies and systems (79–87). For example, whereas classical MD simulations of  $\text{CH}_4$  in water predict  $\Delta w(r_c) \approx -1$  kJ/mol (79, 80), ab initio quantum calculations predict a much larger value of  $\Delta w(r_c) \approx -14$  kJ/mol (85). Although these results appear to indicate that hydrophobic interactions are strongly influenced by quantum effects, the classical predictions are more consistent with various sources of experimental evidence (described below).

Ben-Naim (88) has suggested a beautifully simple and powerful experimentally based means of quantifying water-mediated hydrophobic interactions by, for example, comparing the hydration free energies of methane and ethane, or *para*- and *ortho*-xylene (Figure 7a). He used this procedure to determine that bringing two methyl groups to a separation equal to a covalent CC bond distance of 0.154 nm is associated with a large attractive water-mediated free energy,  $\Delta w \approx -10$  kJ/mol (88). On the other hand, a significantly smaller water-mediated free energy,  $\Delta w \approx -1.3$  kJ/mol

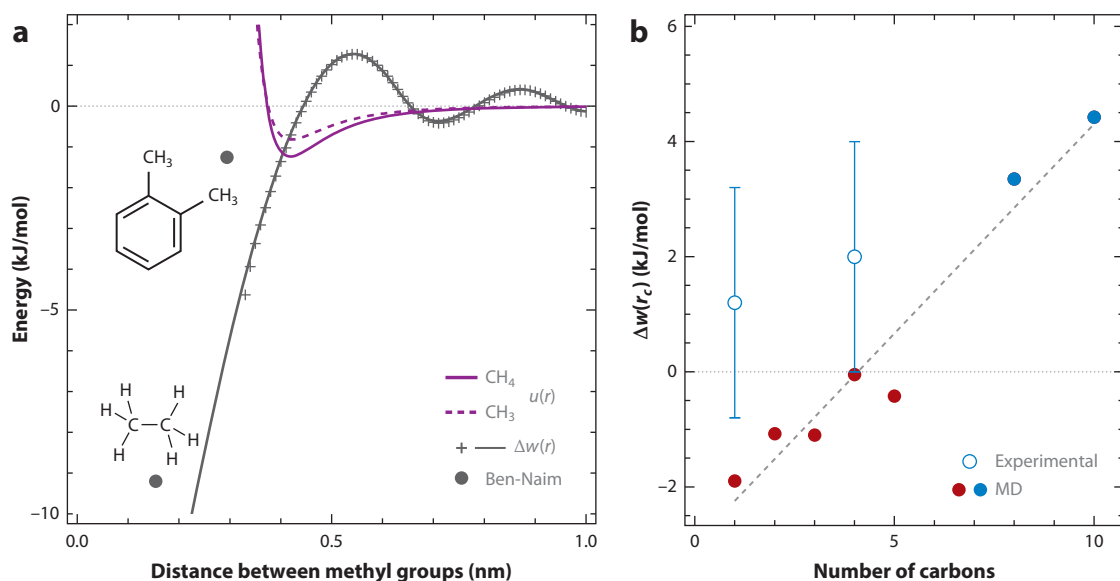


**Figure 7**

(a) Interaction energy of methane ( $\text{CH}_4$ ) molecules (or methyl groups) in the gas phase (purple curves), obtained using classical (TraPPE) potentials (92), compared with Ben-Naim's experimentally derived water-mediated interaction energy of two methyl groups in ethane (89) and in *ortho*-xylene (90) (gray dots). The lower gray dot was obtained from the difference between the experimental hydration  $\Delta G$  of ethane and two methane molecules (89); the upper gray dot was obtained from the difference between the experimental hydration  $\Delta G$  of *ortho*- and *para*-xylene (90). The calculated water-mediated interaction free energy of two  $\text{CH}_4$  molecules (gray curve and plus signs) was obtained using classical (OPLS-UA/TI4P-2005) simulations (79,80). (b) Water-mediated contact free energy obtained from classical (AMBER/TIP3P) simulations (filled dots) of various nonpolar solutes (from  $\text{CH}_4$  to adamantane,  $\text{C}_{10}\text{H}_{16}$ ) (83) and experimental values (open dots) obtained from measurements of aqueous methanol and *tert*-butyl alcohol using Raman–multivariate curve resolution and femtosecond-infrared anisotropy (101). The colors of the points indicate whether the water-mediated contact free energy  $\Delta w$  is attractive (red) or repulsive (blue). Abbreviation: MD, molecular dynamics.

(90), is associated with moving the *para*-methyl groups of xylene to the *ortho* position (at a separation of 0.294 nm). Such experimentally derived results, as well as those obtained by Wu & Prausnitz (91) using Ben-Naim's strategy (88–90), confirm that water-mediated hydrophobic interactions are strongly dependent on the separation between the contacting methyl groups, in qualitative agreement with MD simulations of the water-mediated interaction  $\Delta w(r)$  between CH<sub>4</sub> molecules (**Figure 7a**) (79, 80).

Methyl groups of *ortho*-xylene are significantly closer together than the van der Waals energy minimum for two methyl groups (at  $r \approx 0.42$  nm) (**Figure 7a**) (92). Extrapolation of the experimental points in **Figure 7a** to a value of  $r \approx 0.42$  nm suggests that the water-mediated interaction between two methyl groups in van der Waals contact should be positive (repulsive), thus implying that water opposes rather than drives the formation of such methyl-methyl van der Waals contacts. The differences between the experimental and classical MD results in **Figure 7a** may in part reflect differences between the attraction of water to a CH<sub>4</sub> molecule and a methyl (CH<sub>3</sub>) group. This conclusion is supported by the good agreement between experimental and classical MD simulation results for the hydration energy of methane and ethane (39, 93) (see **Figure 2c**) as well as by more recent classical MD simulation results performed using updated water-water (TIP4P-2005) (94), oil-oil (TraPPE) (92, 95), and oil-water (TIP4P-2005/TraPPE) (93) interaction potentials, which accurately reproduce the experimental hydration free energy difference between *para*- and *ortho*-xylene (H. S. Ashbaugh, private communication).

Further evidence regarding water-mediated hydrophobic interactions is provided, for example, by numerous experimental studies of aqueous *tert*-butyl alcohol (TBA), including neutron scattering (96, 97), light scattering (98, 99), nuclear magnetic resonance (100), and vibrational spectroscopic (101–104) measurements, all indicating that there is little aggregation of TBA below  $\sim 1$  M. Moreover, a recent comparison of aqueous TBA experimental (Raman–multivariate curve resolution and femtosecond-infrared anisotropy) results with random mixing predictions has revealed that the number of free (nonaggregated) TBA molecules is comparable to that expected in a random mixture, and thus is too small to compete with random thermal energy fluctuations ( $RT \approx 2.4$  kJ/mol) (101). More quantitatively, these results imply that the mean force potential between TBA molecules in water may be very slightly attractive, with an average contact free energy of  $w(r_c) \approx -0.6 \pm 2$  kJ/mol (101). The fact that this contact free energy is smaller than the estimated direct (average) contact energy of the nonpolar groups of TBA,  $u(r_c) \approx -2.6$  kJ/mol (see the **Supplemental Appendix**), implies a positive TBA water-mediated contact free energy of  $\Delta w(r_c) \approx 2 \pm 2$  kJ/mol (**Figure 7b**). A similarly obtained estimate of  $\Delta w(r_c) \approx 1.2 \pm 2$  is found for methanol contacts in water, given that  $w(r_c) \approx +0.4 \pm 2$  (1, 101) and  $u(r_c) \approx -0.8$  kJ/mol (**Figure 7b**) (see also the **Supplemental Appendix**). The positive sign of these experimentally derived contact values of  $\Delta w$  (like the extrapolation of the Ben-Naim points in **Figure 7a** to van der Waals contact separations) imply that water-mediated interactions drive hydrophobic groups apart rather than push them together (1).

The above results suggest that water-mediated contact free energies between pairs of small oily groups are typically repulsive. However, the total mean force potential  $w(r)$  between oily groups may nevertheless have an attractive well depth, as  $w(r)$  is equal to the sum of a negative direct interaction,  $u(r)$ , and a positive water-mediated interaction,  $\Delta w(r)$ . Moreover, the self-assembly of micelles (105–107), as well as hydrophobic host-guest complexes (25–31), implies that the associated attractive potential of mean force has a contact well depth that exceeds thermal energy fluctuations. However, the magnitude (and even the sign) of  $\Delta w$  for such processes, and particularly its dependence on the size of the oily molecules, has yet to be definitively determined. The results described in Section 3.2 lead to the rather surprising conclusion that water-mediated interactions become increasingly repulsive as the size of the interacting oily groups increase.

 [Supplemental Material](#)

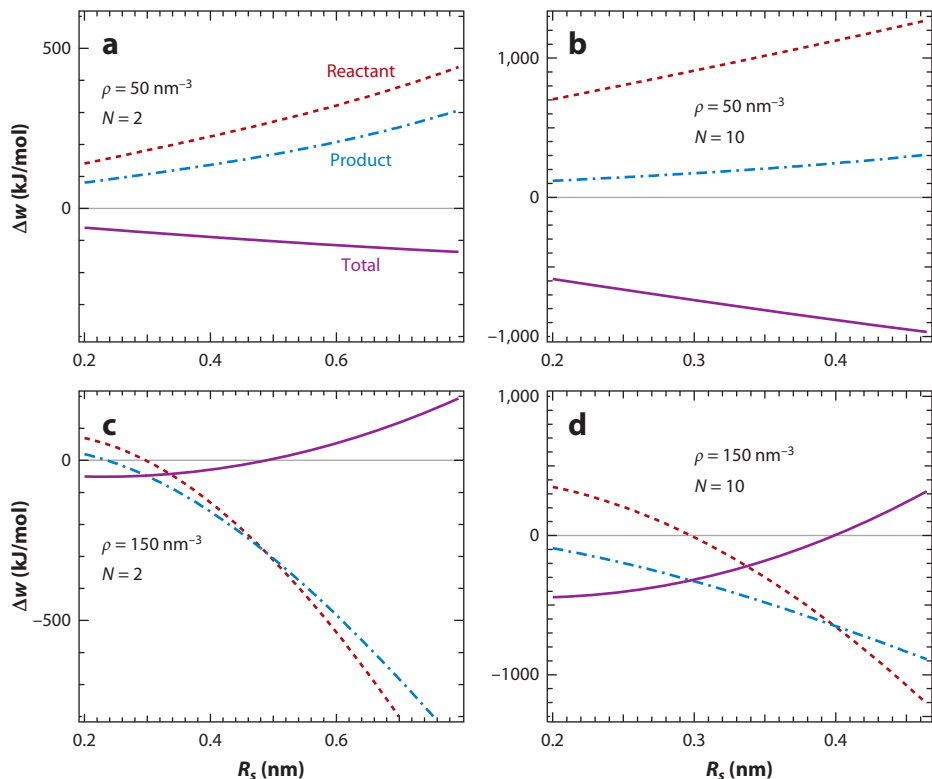


**Figure 8**

Water-mediated free energy of droplet coalescence reactions, in which  $N$  separate spherical drops of radius  $R_s$  and methyl group number density  $\rho$  combine to form a single spherical drop, obtained using classical (OPLS-UA/TIP4P) simulations (48). Shown are the resulting hydration free energies of the reactant (*dashed curves*) and product (*dot-dashed curves*) oil drops and the resulting water-mediated coalescence free energy (*solid curves*) plotted as a function of the reactant oil-drop radius  $R_s$  for the coalescence of either  $N = 2$  (*right column*) or  $N = 10$  (*left column*) oil drops with methyl group densities of either  $\rho = 50 \text{ nm}^{-3}$  (*top row*) or  $\rho = 150 \text{ nm}^{-3}$  (*bottom row*).

However, the attractive direct interaction between the oily groups (which also increases with size) may win the tug-of-water to produce a slightly attractive total potential of mean force.

### 3.2. The Influence of Solute Size and Attractions

Oil-drop hydration results (such as those shown in **Figures 5** and **6**) offer some clues regarding the expected size dependence of water-mediated interactions. More specifically, these results may be used to predict water-mediated contributions to oil-drop coalescence reactions, in which  $N$  oil drops of radius  $R_s$  combine to form a larger oil drop of radius  $R_s N^{1/3}$ . **Figure 8** shows the hydration free energies of the reactant and product oil drops as well as the resultant water-mediated coalescence free energy, plotted as a function of the reactant oil-drop radius  $R_s$ .

The results shown in **Figure 8a,b** reveal that the water-mediated interactions between moderately hydrophobic (weakly attractive) oil drops invariably favor oil-drop coalescence (aggregation), with a free energy driving force that increases with oil-drop size. Note that these water-mediated

coalescence free energies do not include the direct interaction between the oil molecules (which would further favor aggregation). On the other hand, the results shown in **Figure 8c,d**, which pertain to oil drops with a somewhat stronger (van der Waals) attraction to water, have a more interesting dependence on oil-drop size, as  $\Delta w$  changes sign with increasing  $R_s$  (in a way that depends on both  $N$  and  $\rho$ ). This rather counterintuitive behavior implies that water-mediated interactions drive small oil drops to aggregate ( $\Delta w < 0$ ) but favor the breakup of large oil drops ( $\Delta w > 0$ ).

The results shown in **Figure 7b**, which pertain to the aggregation of nearly spherical hydrocarbon molecules (rather than idealized oil drops), imply that the attraction-induced crossover behavior seen in **Figure 8** may be quite general (1, 83, 84, 108, 109). More specifically, the classical MD simulation results shown in **Figure 7b** predict that the water-mediated free energy associated with bringing two hydrocarbon molecules into contact with each other is negative (attractive) for  $\text{CH}_4$  and other nearly spherical molecules as large as neopentane ( $\text{C}_5\text{H}_{12}$ ) but becomes positive (repulsive) for larger molecules such as adamantane ( $\text{C}_{10}\text{H}_{26}$ ) (83). This conclusion is also consistent with classical MD results obtained for larger carbon clusters including buckminsterfullerene  $\text{C}_{60}$  (83, 84, 108, 109). In other words, such predictions imply that the water-mediated interaction between small oily molecules is attractive, thus favoring hydrophobic aggregation, but becomes repulsive for larger oily molecules, thus driving them apart (1). However, the MD predictions (**Figure 7b**) are invariably somewhat smaller (more attractive) than the corresponding experimentally derived results (see Section 3.1) (1, 101). It remains unclear if this discrepancy reflects inaccuracies of the classical MD potentials or is due to the fact that the experimental points pertain to water-mediated hydrophobic interactions between alcohols whereas the MD results pertain to alkanes. The former explanation may be more likely, as recent comparisons of classical MD predictions and experimental (Raman–multivariate curve resolution and femtosecond-infrared anisotropy), both pertaining to aqueous TBA, indicate that simulation results obtained using classical (OPLS-AA/TIP4P) potential functions predict slightly more aggregation than observed experimentally (101).

### 3.3. Second Virial Coefficients in Water and the Gas Phase

An additional source of both theoretical and experimental evidence pertaining to water-mediated hydrophobic interactions may be obtained from second virial coefficients,  $B_2$ , which quantify nonideal contributions to the pressure, or osmotic pressure, of gases and solutions. For example, a hard-sphere gas has a positive  $B_2$  that is equivalent to the excluded volume due to pairwise contacts. By contrast, attractive interactions lead to a volume decrease and thus contribute negatively to  $B_2$  (110, 111). More specifically, in the gas phase  $B_2 = -\frac{1}{2} \int [e^{-\beta u(r)} - 1] 4\pi r^2 dr$ , whereas in water  $B_2 = -\frac{1}{2} \int [e^{-\beta w(r)} - 1] 4\pi r^2 dr$  (both pertaining to the infinitely dilute solute limit). Note that the latter expression for the osmotic  $B_2$  may also be used to obtain the gas phase  $B_2$ , as  $w(r) = u(r)$  in the absence of a solvent.

Osmotic second virial coefficients are notoriously difficult to calculate because they are sensitive to subtle long-range correlations, related to the oscillations in  $\Delta w(r)$  shown in **Figure 7a** (which are amplified by the  $r^2$  weighting of the  $B_2$  integrand). Nevertheless various procedures have been developed to deal with the numerical difficulties associated with obtaining  $B_2$  predictions from MD simulations (24, 79, 80, 112). The results, such as those shown in **Figure 9**, again confirm the critical role of solute-water attractions in damping hydrophobic interactions and even in changing their sign.

The results shown in **Figure 9a** indicate that the water-mediated contribution to  $B_2$  is predicted to be repulsive ( $B_2 > 0$ ) at ambient (and lower) temperature but to become attractive ( $B_2 < 0$ ) at high temperatures (1, 80). Hard spheres (of comparable size to  $\text{CH}_4$ ) are predicted to have

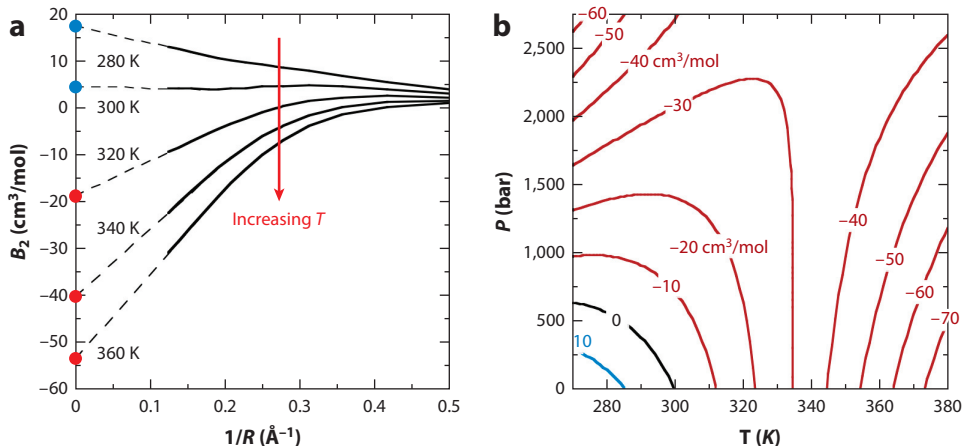


**Figure 9**

Methane osmotic second virial coefficient ( $B_2$ ) results obtained using classical (OPSL-UA/TIP4P-2005) simulations (79). (a) Points on the left-hand axis mark the  $B_2$  extrapolated from integrals of the methane-water radial distribution function over various integration ranges ( $R$ ). (b) Contour plot showing the predicted temperature and pressure dependence of the osmotic second virial coefficient of methane. The colors of the (a) points and (b) curves indicate whether  $B_2$  is attractive (red) or repulsive (blue). Figure adapted from Reference 79 with permission. Copyright 2015 American Chemical Society.

substantially more attractive  $B_2$  values but a similar temperature dependence (24). The  $B_2$  of Xe in water has also been predicted to decrease (become more negative) with increasing temperature (51). This temperature dependence is quite remarkable, as it is opposite to that in the gas phase, where  $B_2$  is invariably negative at low temperatures, owing to the long-range intermolecular attractive interactions, and increases with increasing temperature, eventually becoming positive as a result of short-range repulsive-core interactions (111, 113).

**Figure 9b** shows classical MD predictions of the temperature and pressure dependence of the osmotic  $B_2$  of  $\text{CH}_4$ , revealing that  $\text{CH}_4$  aggregation is favored ( $B_2 < 0$ ) at both high pressures and temperatures but disfavored ( $B_2 > 0$ ) at lower, near ambient temperatures and pressures. The prediction that  $B_2 > 0$  for  $\text{CH}_4$  at ambient (and lower) temperatures is consistent with the expectation that the hydration shell of  $\text{CH}_4$  is most stable in this regime. The latter conclusion is also consistent with the low temperature formation of clathrate hydrates composed of  $\text{CH}_4$  (or other small and relatively nonpolar molecules) completely surrounded by an H-bonded cage of water molecules (114–118) as well as with spectroscopic results revealing that the number of broken H-bonds (free OH groups) in hydrophobic hydration shells decreases with decreasing temperature (53, 119, 120). Moreover, as pointed out long ago by Clark et al. (121), comparisons of the gas phase and osmotic second virial coefficients of alkanes and alcohols imply that the water-mediated contributions to  $B_2$  are positive (as the gas-phase  $B_2$  values of alkanes are more negative than the osmotic  $B_2$  values of the alcohols with the same aliphatic groups) (19, 121). Similarly, the osmotic  $B_2$  of other nonpolar and amphiphilic solutes increases (becomes less negative) with increasing temperature (19, 122) as well as with increasing solute size (19, 121, 123). Thus, it is hard to avoid the conclusion that water-mediated interactions between oily molecules become more repulsive with decreasing temperature and increasing solute size.

However, as a cautionary tale and illustration of the difficulties associated with accurately measuring or predicting  $B_2$ , recent MD simulations obtained an osmotic second virial coefficient of  $B_2 \approx -40.9 \text{ cm}^3/\text{mol}$  for propane in water, whereas two different equation of state based

predictions yielded  $B_2$  values that are more than 10 times larger in magnitude (124). Although such huge discrepancies have yet to be explained, they may perhaps be influenced by the fact that the simulations were performed on an aqueous solution with a propane mole fraction of  $\chi = 6 \times 10^{-3}$ , which is 200 times the experimental equilibrium solubility ( $\chi = 2.7 \times 10^{-5}$ ) of propane in water at 298 K, thus raising the possibility that these and other  $B_2$  simulation results may be influenced by the metastability of the simulated systems (124). Alternatively, the above discrepancies may be linked to errors associated with the analytical mixture equation of state extrapolations. More generally, errors in the apparent value of  $B_2$  may arise either from the presence of long-range two-body correlations or from the influence of higher-order multibody correlations (of either short or long range) that remain non-negligible at the concentration under which simulations (or experimental measurements) are performed.

#### 4. DISCUSSION AND OUTLOOK

The delicate balance of repulsive (entropic) and attractive (energetic) oil-water interactions situates oily molecules near a hydrophathic precipice, along which water-mediated interactions do not far exceed thermal energy fluctuations—this fortunate situation makes hydrophobic interactions useful in the self-assembly of organisms and devices that must possess both structural integrity and dynamic reactivity. The attractive water-mediated interaction  $\Delta w$  between purely repulsive hydrophobic (hard-sphere) solutes is strongly damped by the introduction of oil-water attractive interactions. Although open questions remain regarding the precise dependence of  $\Delta w$  on solute size and shape, mounting evidence suggests that the total potential of mean force  $w = u + \Delta w$  between contacting oily molecules is slightly attractive, with a magnitude that exceeds thermal energy fluctuations only when a sufficiently large amount of water-exposed hydrophobic surface area is buried upon binding. For example, analysis of a wide range of both biological and synthetic host-guest binding processes indicates that the corresponding binding free energy  $\Delta G = \Delta w = -RT \ln K_A$  exceeds thermal energy ( $\Delta G < -RT$ ) only when more than  $\sim 0.8 \pm 0.3 \text{ nm}^2$  of solvent-exposed surface area is buried upon binding (27). Although the latter surface area threshold is significantly larger than the value of  $\sim 0.023 \text{ nm}^2$  inferred from classical MD simulations of small-molecule hydrophobic contacts (125), it is in better agreement with the rough estimate of  $\sim 1 \text{ nm}^2$  inferred from recent spectroscopic measurements of alcohol aggregation processes (1, 101). Further simulations performed using recently developed theoretical strategies (82, 112, 126, 127) and potential functions (92, 93, 95) may hold the key to resolving the remaining discrepancies between experimental and MD results.

Hydrophobic hydration and interaction processes are often found to display substantial enthalpy-entropy compensation. This must be due, at least in part, to the exact compensation of solvent-reorganization interactions associated with solute-induced changes in the number and strength of water-water H-bonds. The strong temperature dependence of this compensating water-reorganization enthalpy is evidently responsible for the characteristically large hydration heat capacities of oily molecules (44). However, the energy and entropy arising from direct oil-water interactions (which need not compensate) also happen to be almost perfectly compensating, owing to the apparently accidental near equality of cavity formation ( $TS_{UV}$ ) and oil-water van der Waals ( $E_{UV}$ ) contributions to alkane hydration free energies ( $\Delta G$ ).

Much has been made of the enthalpic (“nonclassical”) hydrophobic effect exhibited by some host-guest binding processes, which appear to be enthalpically rather than entropically dominated (29, 30, 128–130). This behavior has been attributed to the release of weakly H-bonded water molecules into the more strongly H-bonded bulk (26, 130, 131). Similar arguments have been invoked to explain the striking correlation between hydrophobic host-guest binding free energies

and the release of “high-energy” water molecules (129, 132) as well as to explain the repulsive water-mediated interactions between larger nonpolar molecules such as  $C_{60}$  (83, 109). However, such arguments have not taken into account the compensation of water-reorganization enthalpy and entropy (required by Equations 2–4). This exact compensation is linked to the fact that the partial molar free energies (chemical potential) of all water molecules in any equilibrium solution are all necessarily the same, which requires that there be no free energy difference between a water molecule in a host cavity (or a hydrophobic hydration shell) and the surrounding bulk water molecules (133). Although the enthalpy and entropy of hydrophobic hydration-shell (or cavity-bound) waters may differ greatly from bulk water, their free energies cannot. Therefore, the associated enthalpy and entropy differences must exactly compensate. Thus, the free energy driving force for host-guest binding and hydrophobic aggregation cannot be attributed free energy differences between interfacial and bulk water, but rather it must be explained in terms of aggregation-induced changes in the direct interactions between water and the oily molecules.

As first suspected by Kauzmann (17), subsequently demonstrated by Stillinger (21), and significantly elaborated upon by Lum and coworkers (22), hydrophobicity is expected to depend critically on the size (or curvature) of an oily molecule (or interface). The resulting hydrophobic crossover phenomena has been observed in MD simulations (11, 20, 33, 134, 135), and similar crossover behavior has been observed in recent single-molecule polymer-unfolding (136–138) and hydration-shell spectroscopic measurements (53, 139). The present review highlights another sort of hydrophobic crossover—one induced by oil-water attractive interactions (76, 86, 140, 141). As a result, water-mediated interactions between large oily molecules are predicted to be repulsive, not only for model oil-drop coalescence processes (48) (as shown in **Figure 8**), but also for nearly spherical hydrocarbons (83) and alcohols (1, 101) (as shown in **Figure 7b**) as well as for host-guest binding processes (142). Moreover, recent studies of the aggregation of aqueous alcohols (101) suggest that water-mediated interactions between oily molecules may be somewhat more repulsive than predicted by classical MD simulations (as shown, for example, in **Figure 7b**) (1).

In addition to the above issues, open questions remain regarding the influence of cooperativity on hydrophobic interactions (85, 117, 143–150), where cooperativity is defined as the difference between  $\Delta w(\tau)$  for the aggregation of a collection of  $N$  oily molecules and the sum of the water-mediated interactions between each pair of molecules in the aggregate. In general, such multibody water-mediated interactions may be either cooperative or anticooperative, depending on whether  $\Delta w(\tau)$  of the aggregate is greater or less than the sum of the corresponding pairwise water-mediated interactions. For example, the oil-drop coalescence predictions shown in **Figure 8** imply significant anticooperativity, as  $\Delta w$  for the coalescence of  $N = 10$  oil drops is invariably much smaller than  $\frac{1}{2}N(N - 1) = 45$  times  $\Delta w$  for the coalescence of  $N = 2$  oil drops (of the same size and methyl group density), where  $\frac{1}{2}N(N - 1)$  is the number of unique pairs in a collection of  $N$  identical objects. Simulations of various other hydrophobic aggregation processes have uncovered both cooperative and anticooperative behavior, depending on the shapes and arrangements of the aggregating solute molecules (145, 146), as well as temperature and concentration (149). It remains to be determined if micelle formation and other biologically important self-assembly processes, such as the formation of cell membranes, vesicles, and virus capsids, are cooperative or anticooperative in the above sense, as anticooperative processes may nevertheless be strongly driven to aggregate (as exemplified by the oil-drop coalescence results shown in **Figure 8**).

## DISCLOSURE STATEMENT

The author is not aware of any affiliations, memberships, funding, or financial holdings that might be perceived as affecting the objectivity of this review.

## ACKNOWLEDGMENTS

This work was supported by the National Science Foundation (CHE-1213338). Robin Underwood generated the oil-drop MD simulation results used to produce **Figures 5, 6, and 8**, as described in the **Supplemental Appendix** and Reference 48. Hank Ashbaugh kindly provided some of the published (79) and unpublished results shown in **Figures 7 and 9**. Discussions with Ben Widom, David Chandler, Lawrence Pratt, Hank Ashbaugh, Amish Patel, Monte Pettitt, Bruce Gibb, and Blake Rankin contributed to shaping this review.

 Supplemental Material

## LITERATURE CITED

1. Ben-Amotz D. 2015. Hydrophobic ambivalence: teetering on the edge of randomness. *J. Phys. Chem. Lett.* 6:1696–701
2. Willard AP. 2015. Illuminating the interactions between small solutes in liquid water. *J. Phys. Chem. Lett.* 6:1616–17
3. Schrodinger E. 1944. *What Is Life?* Cambridge, UK: Cambridge Univ. Press
4. Pohorille A, Pratt LR. 2012. Is water the universal solvent for life? *Orig. Life Evol. Biosph.* 42:405–9
5. Ball P. 2008. Water as an active constituent in cell biology. *Chem. Rev.* 108:74–108
6. Lynden-Bell RM, Giovambattista N, Debenedetti PG, Head-Gordon T, Rossky PJ. 2011. Hydrogen bond strength and network structure effects on hydration of non-polar molecules. *Phys. Chem. Chem. Phys.* 13:2748–57
7. Willard AP, Chandler D. 2014. The molecular structure of the interface between water and a hydrophobic substrate is liquid-vapor like. *J. Chem. Phys.* 141:18C519
8. Baldwin RL. 2014. Dynamic hydration shell restores Kauzmann's 1959 explanation of how the hydrophobic factor drives protein folding. *PNAS* 111:13052–56
9. Patel AJ, Varilly P, Jamadagni SN, Hagan MF, Chandler D, Garde S. 2012. Sitting at the edge: how biomolecules use hydrophobicity to tune their interactions and function. *J. Phys. Chem. B* 116:2498–503
10. Sharp KA, Vanderkooi JM. 2010. Water in the half shell: structure of water, focusing on angular structure and solvation. *Acc. Chem. Res.* 43:231–39
11. Ashbaugh HS, Pratt LR. 2006. Colloquium: scaled particle theory and the length scales of hydrophobicity. *Rev. Mod. Phys.* 78:159–78
12. Southall NT, Dill KA, Haymet ADJ. 2002. A view of the hydrophobic effect. *J. Phys. Chem. B* 106:521–33
13. Muller N. 1990. Search for a realistic view of the hydrophobic effect. *Acc. Chem. Res.* 23:23–28
14. Pratt LR, Chandler D. 1986. Theoretical and computational studies of hydrophobic interactions. *Methods Enzymol.* 127:48–63
15. Tanford C. 1978. Hydrophobic effect and organization of living matter. *Science* 200:1012–18
16. Tanford C. 1980. *The Hydrophobic Effect: Formation of Micelles and Biological Membranes*. New York: Wiley
17. Kauzmann W. 1959. Some factors in the interpretation of protein denaturation. *Adv. Protein Chem.* 14:1–63
18. Frank HS, Evans JW. 1945. Free volume and entropy in condensed systems. 3. Entropy in binary liquid mixtures; partial molar entropy in dilute solutions: structure and thermodynamics of aqueous electrolytes. *J. Chem. Phys.* 13:507–32
19. Blokzijl W, Engberts JBFN. 1993. Hydrophobic effects: opinions and facts. *Angew. Chem. Int. Ed.* 32:1545–79
20. Chandler D. 2005. Interfaces and the driving force of hydrophobic assembly. *Nature* 437:640–47
21. Stillinger FH. 1973. Structure in aqueous solutions of nonpolar solutes from the standpoint of scaled-particle theory. *J. Solut. Chem.* 2:141–58
22. Lum K, Chandler D, Weeks JD. 1999. Hydrophobicity at small and large length scales. *J. Phys. Chem. B* 103:4570–77
23. Hummer G, Garde S, Garcia AE, Paulaitis ME, Pratt LR. 1998. Hydrophobic effects on a molecular scale. *J. Phys. Chem. B* 102:10469–82

24. Chaudhari MI, Holleran SA, Ashbaugh HS, Pratt LR. 2013. Molecular-scale hydrophobic interactions between hard-sphere reference solutes are attractive and endothermic. *PNAS* 110:20557–62
- 24a. Harris RC, Pettitt BM. 2016. Reconciling the understanding of ‘hydrophobicity’ with physics-based models of proteins. *J. Phys. Condens. Matter* 28:083003
- 24b. Harris RC, Pettitt BM. 2014. Effects of geometry and chemistry on hydrophobic solvation. *PNAS* 111:14681–86
- 24c. Harris RC, Drake JA, Pettitt BM. 2014. Multibody correlations in the hydrophobic solvation of glycine peptides. *J. Chem. Phys.* 141:22D525
25. Jordan JH, Gibb BC. 2015. Molecular containers assembled through the hydrophobic effect. *Chem. Soc. Rev.* 44:547–85
26. Baron R, McCammon JA. 2013. Molecular recognition and ligand association. *Annu. Rev. Phys. Chem.* 64:151–75
27. Houk KN, Leach AG, Kim SP, Zhang XY. 2003. Binding affinities of host-guest, protein-ligand, and protein-transition-state complexes. *Angew. Chem. Int. Ed.* 42:4872–97
28. Rasaiah JC, Garde S, Hummer G. 2008. Water in nonpolar confinement: from nanotubes to proteins and beyond. *Annu. Rev. Phys. Chem.* 59:713–40
29. Hummer G. 2010. Molecular binding under water’s influence. *Nat. Chem.* 2:906–7
30. Abel R, Young T, Farid R, Berne BJ, Friesner RA. 2008. Role of the active-site solvent in the thermodynamics of factor Xa ligand binding. *J. Am. Chem. Soc.* 130:2817–31
31. Hillyer MB, Gibb BC. 2015. Molecular shape and the hydrophobic effect. *Annu. Rev. Phys. Chem.* 67. In press
32. Jamadagni SN, Godawat R, Garde S. 2011. Hydrophobicity of proteins and interfaces: insights from density fluctuations. *Annu. Rev. Chem. Biomol. Eng.* 2:147–71
33. Berne BJ, Weeks JD, Zhou RH. 2009. Dewetting and hydrophobic interaction in physical and biological systems. *Annu. Rev. Phys. Chem.* 60:85–103
34. Ben-Naim A. 1987. *Solvation Thermodynamics*. New York: Plenum
35. Ben-Naim A. 1978. Standard thermodynamics of transfer. Uses and misuses. *J. Phys. Chem.* 82:792–803
36. Underwood R, Tomlinson-Phillips J, Ben-Amotz D. 2010. Are long-chain alkanes hydrophilic? *J. Phys. Chem. B* 114:8646–51
37. Ben-Amotz D, Underwood R. 2008. Unraveling water’s entropic mysteries: a unified view of nonpolar, polar, and ionic hydration. *Acc. Chem. Res.* 41:957–67
38. Plyasunova NV, Plyasunov AV, Shock EL. 2004. Database of thermodynamic properties for aqueous organic compounds. *Int. J. Thermophys.* 25:351–60
39. Gallicchio E, Kubo MM, Levy RM. 2000. Enthalpy-entropy and cavity decomposition of alkane hydration free energies: numerical results and implications for theories of hydrophobic solvation. *J. Phys. Chem. B* 104:6271–85
40. Duffy EM, Jorgensen WL. 2000. Prediction of properties from simulations: free energies of solvation in hexadecane, octanol, and water. *J. Am. Chem. Soc.* 122:2878–88
41. Ferguson AL, Debenedetti PG, Panagiotopoulos AZ. 2009. Solubility and molecular conformations of *n*-alkane chains in water. *J. Phys. Chem. B* 113:6405–14
42. Widom B. 1982. Potential distribution theory and the statistical mechanics of fluids. *J. Phys. Chem.* 86:869–72
43. Ben-Amotz D, Raineri F, Stell G. 2005. Solvation thermodynamics: theory and applications. *J. Phys. Chem. B* 109:6866–78
44. Ben-Amotz D, Widom B. 2006. Generalized solvation heat capacities. *J. Phys. Chem. B* 110:19839–49
45. Ben-Naim A. 1978. A simple model for demonstrating the relation between solubility, hydrophobic interaction, and structural changes in the solvent. *J. Phys. Chem.* 82:874–85
46. Yu HA, Karplus M. 1988. A thermodynamic analysis of solvation. *J. Chem. Phys.* 89:2366–79
47. Raineri FO, Stell G, Ben-Amotz D. 2005. New mean-energy formulae for free energy differences. *Mol. Phys.* 103:3209–21
48. Underwood R, Ben-Amotz D. 2011. Communication: length scale dependent oil-water energy fluctuations. *J. Chem. Phys.* 113:201102

49. Lemmon EW, Perkins AP, McLinden MO, Friend DG. 2000. *NIST Standard Reference Database 12*, Version 5.0. Boulder: Natl. Inst. Stand. Technol.
50. Gallagher KR, Sharp KA. 2003. A new angle on heat capacity changes in hydrophobic solvation. *J. Am. Chem. Soc.* 125:9853–60
51. Paschek D. 2004. Temperature dependence of the hydrophobic hydration and interaction of simple solutes: an examination of five popular water models. *J. Chem. Phys.* 120:6674–90
52. Paschek D. 2004. Heat capacity effects associated with the hydrophobic hydration and interaction of simple solutes: a detailed structural and energetical analysis based on molecular dynamics simulations. *J. Chem. Phys.* 120:10605–17
53. Davis JG, Gierszal KP, Wang P, Ben-Amotz D. 2012. Water structural transformation at molecular hydrophobic interfaces. *Nature* 491:582–85
54. Ben-Amotz D. 2005. Global thermodynamics of hydrophobic cavitation, dewetting, and hydration. *J. Chem. Phys.* 123:184504
55. Makhatadze GI, Privalov PL. 1988. Partial specific-heat capacity of benzene and of toluene in aqueous solution determined calorimetrically for a broad temperature-range. *J. Chem. Thermodyn.* 20:405–12
56. Dohnal V, Fenclova D, Vrbka P. 2006. Temperature dependences of limiting activity coefficients, Henry's law constants, and derivative infinite dilution properties of lower ( $C_1$ – $C_5$ ) 1-alkanols in water. Critical compilation, correlation, and recommended data. *J. Phys. Chem. Ref. Data* 35:1621–51
57. Makhatadze GI, Lopez MM, Privalov PL. 1997. Heat capacities of protein functional groups. *Biophys. Chem.* 64:93–101
58. Pollack GL, Himm JF. 1982. Solubility of xenon in liquid *n*-alkanes: temperature dependence and thermodynamic functions. *J. Chem. Phys.* 77:3221–29
59. Pollack GL, Kennan RP, Himm JF, Carr PW. 1989. Solubility of xenon in 45 organic solvents including cycloalkanes, acids, and alkanols: experiment and theory. *J. Chem. Phys.* 90:6569–79
60. Angell CA, Oguni M, Sichina WJ. 1982. Heat capacity of water at extremes of supercooling and superheating. *J. Phys. Chem.* 86:998–1002
61. Wheeler JC. 1972. Behavior of a solute near critical point of an almost pure solvent. *Ber. Bunsenges. Phys. Chem.* 76:308–18
62. Biggerstaff DR, Wood RH. 1988. Apparent molar heat-capacities of aqueous argon, ethylene, and xenon at temperatures up to 720 K and pressures to 33 MPa. *J. Phys. Chem.* 92:1994–2000
63. Gill SJ, Dec SF, Olofsson G, Wadso I. 1985. Anomalous heat capacity of hydrophobic solvation. *J. Phys. Chem.* 89:3758–61
64. Ben-Naim A. 1992. *Statistical Thermodynamics for Chemists and Biochemists*. New York: Plenum
65. Lee B, Graziano G. 1996. A two-state model of hydrophobic hydration that produces compensating enthalpy and entropy changes. *J. Am. Chem. Soc.* 118:5163–68
66. Holten V, Palmer JC, Poole PH, Debenedetti PG, Anisimov MA. 2014. Two-state thermodynamics of the ST2 model for supercooled water. *J. Chem. Phys.* 140:014502
67. Russo J, Tanaka H. 2014. Understanding water's anomalies with locally favoured structures. *Nat. Commun.* 5:3556
68. Palmer JC, Martelli F, Liu Y, Car R, Panagiotopoulos AZ, Debenedetti PG. 2014. Metastable liquid-liquid transition in a molecular model of water. *Nature* 510:385–88
69. Limmer DT, Chandler D. 2013. The putative liquid-liquid transition is a liquid-solid transition in atomistic models of water. II. *J. Chem. Phys.* 138:214504
70. Giovambattista N, Loerting T, Lukanov BR, Starr FW. 2012. Interplay of the glass transition and the liquid-liquid phase transition in water. *Sci. Rep.* 2:390
71. Seidl M, Fayter A, Stern JN, Zifferer G, Loerting T. 2015. Shrinking water's no man's land by lifting its low-temperature boundary. *Phys. Rev. B* 91:144201
72. Cheng YK, Rossky PJ. 1998. Surface topography dependence of biomolecular hydrophobic hydration. *Nature* 392:696–99
73. Friesen AD, Matyushov DV. 2011. Non-Gaussian statistics of electrostatic fluctuations of hydration shells. *J. Chem. Phys.* 135:104501

74. Geissler PL. 2005. Temperature dependence of inhomogeneous broadening: on the meaning of isosbestic points. *J. Am. Chem. Soc.* 127:14930–35
75. Smith JD, Cappa CD, Wilson KR, Cohen RC, Geissler PL, Saykally RJ. 2005. Unified description of temperature-dependent hydrogen-bond rearrangements in liquid water. *PNAS* 102:14171–74
76. Huang DM, Chandler D. 2002. The hydrophobic effect and the influence of solute-solvent attractions. *J. Phys. Chem. B* 106:2047–53
77. Chandler D, Weeks JD, Andersen HC. 1983. van der Waals picture of liquids, solids, and phase-transformations. *Science* 220:787–94
78. Remsing RC, Patel AJ. 2015. Water density fluctuations relevant to hydrophobic hydration are unaltered by attractions. *J. Chem. Phys.* 142:024502
79. Ashbaugh HS, Weiss K, Williams SM, Meng B, Surampudi LN. 2015. Temperature and pressure dependence of methane correlations and osmotic second virial coefficients in water. *J. Phys. Chem. B* 119:6280–94
80. Koga K. 2013. Osmotic second virial coefficient of methane in water. *J. Phys. Chem. B* 117:12619–24
81. Gupta R, Patey GN. 2012. Aggregation in dilute aqueous *tert*-butyl alcohol solutions: insights from large-scale simulations. *J. Chem. Phys.* 137:034509
82. Ghosh MK, Uddin N, Choi CH. 2012. Hydrophobic and hydrophilic associations of a methanol pair in aqueous solution. *J. Phys. Chem. B* 116:14254–60
83. Makowski M, Czaplewski C, Liwo A, Scheraga HA. 2010. Potential of mean force of association of large hydrophobic particles: toward the nanoscale limit. *J. Phys. Chem. B* 114:993–1003
84. Morrone JA, Li J, Berne BJ. 2012. Interplay between hydrodynamics and the free energy surface in the assembly of nanoscale hydrophobes. *J. Phys. Chem. B* 116:378–89
85. Li JL, Car R, Tang C, Wingreen NS. 2007. Hydrophobic interaction and hydrogen-bond network for a methane pair in liquid water. *PNAS* 104:2626–30
86. Smith DE, Haymet ADJ. 1993. Free-energy, entropy, and internal energy of hydrophobic interactions: computer simulations. *J. Chem. Phys.* 98:6445–54
87. Chaudhari MI, Pratt LR, Paulaitis ME. 2010. Communication: direct observation of a hydrophobic bond in loop closure of a capped  $(-\text{OCH}_2\text{CH}_2)_n$  oligomer in water. *J. Chem. Phys.* 133:231102
88. Ben-Naim A. 1980. *Hydrophobic Interactions*. New York: Plenum
89. Yaacobi M, Ben-Naim A. 1974. Solvophobic interaction. *J. Phys. Chem.* 78:175–78
90. Ben-Naim A, Wilf J. 1979. Direct measurement of intra-molecular hydrophobic interactions. *J. Chem. Phys.* 70:771–77
91. Wu JZ, Prausnitz JM. 2008. Pairwise-additive hydrophobic effect for alkanes in water. *PNAS* 105:9512–15
92. Martin MG, Siepmann JI. 1998. Transferable potentials for phase equilibria. 1. United-atom description of *n*-alkanes. *J. Phys. Chem. B* 102:2569–77
93. Ashbaugh HS, Liu LX, Surampudi LN. 2011. Optimization of linear and branched alkane interactions with water to simulate hydrophobic hydration. *J. Chem. Phys.* 135:054150
94. Abascal JLF, Vega C. 2005. A general purpose model for the condensed phases of water: TIP4P/2005. *J. Chem. Phys.* 123:234505
95. Martin MG, Siepmann JI. 1999. Novel configurational-bias Monte Carlo method for branched molecules. Transferable potentials for phase equilibria. 2. United-atom description of branched alkanes. *J. Phys. Chem. B* 103:4508–17
96. Bowron DT, Moreno SD. 2002. The structure of a concentrated aqueous solution of tertiary butanol: water pockets and resulting perturbations. *J. Chem. Phys.* 117:3753–62
97. Bowron DT, Soper AK, Finney JL. 2001. Temperature dependence of the structure of a 0.06 mole fraction tertiary butanol-water solution. *J. Chem. Phys.* 114:6203–19
98. Sedlak M, Rak D. 2013. Large-scale inhomogeneities in solutions of low molar mass compounds and mixtures of liquids: supramolecular structures or nanobubbles? *J. Phys. Chem. B* 117:2495–504
99. Subramanian D, Anisimov MA. 2011. Resolving the mystery of aqueous solutions of tertiary butyl alcohol. *J. Phys. Chem. B* 115:9179–83

100. Sinibaldi R, Casieri C, Melchionna S, Onori G, Segre AL, et al. 2006. The role of water coordination in binary mixtures. A study of two model amphiphilic molecules in aqueous solutions by molecular dynamics and NMR. *J. Phys. Chem. B* 110:8885–92
101. Rankin BM, Ben-Amotz D, van der Post ST, Bakker HJ. 2015. Contacts between alcohols in water are random rather than hydrophobic. *J. Phys. Chem. Lett.* 6:688–92
102. Petersen C, Bakulin AA, Paveleyev VG, Pshenichnikov MS, Bakker HJ. 2010. Femtosecond midinfrared study of aggregation behavior in aqueous solutions of amphiphilic molecules. *J. Chem. Phys.* 133:164514
103. Wilcox DS, Rankin BM, Ben-Amotz D. 2013. Distinguishing aggregation from random mixing in aqueous *t*-butyl alcohol solutions. *Faraday Discuss.* 167:177–90
104. Freda M, Onori G, Santucci A. 2001. Infrared and dielectric spectroscopy study of the water perturbation induced by two small organic solutes. *J. Mol. Struct.* 565:153–57
105. Maibaum L, Dinner AR, Chandler D. 2004. Micelle formation and the hydrophobic effect. *J. Phys. Chem. B* 108:6778–81
106. Wennerstrom H, Lindman B. 1979. Micelles: physical chemistry of surfactant association. *Phys. Rep.* 52:1–86
107. Mukerjee P, Mysels KJ. 1971. *Critical Micelle Concentrations of Aqueous Surfactant Systems*. Washington, DC: Natl. Bur. Stand.
108. Li LW, Bedrov D, Smith GD. 2006. Water-induced interactions between carbon nanoparticles. *J. Phys. Chem. B* 110:10509–13
109. Zangi R. 2014. Are buckyballs hydrophobic? *J. Phys. Chem. B* 118:12263–70
110. Ben-Amotz D, Widom B. 2007. Nonideal gas solvation thermodynamics. *J. Chem. Phys.* 126:104502
111. Ben-Amotz D, Gift AD, Levine RD. 2002. Improved corresponding states scaling of the equations of state of simple fluids. *J. Chem. Phys.* 117:4632–34
112. Chaudhari MI, Sabo D, Pratt LP, Remppe SB. 2014. Hydration of Kr(aq) in dilute and concentrated solutions. *J. Phys. Chem. B* 119:9098–102
113. Hirschfelder JO, Curtiss CF, Bird RB. 1964 (1954). *Molecular Theory of Gases and Liquids*. New York: Wiley
114. Van der Waals JH, Platteeuw JC. 1959. Clathrate solutions. *Adv. Chem. Phys.* 2:1–57
115. Sloan ED. 1998. *Clathrate Hydrates of Natural Gases*. New York: Marcel Dekker
116. Clawson JS, Cygan RT, Alam TM, Leung K, Remppe SB. 2010. Ab initio study of hydrogen storage in water clathrates. *J. Comput. Theor. Nanosci.* 7:2602–6
117. Jacobson LC, Hujo W, Molinero V. 2010. Amorphous precursors in the nucleation of clathrate hydrates. *J. Am. Chem. Soc.* 132:11806–11
118. Ward ZT, Marriott RA, Sum AK, Sloan ED, Koh CA. 2015. Equilibrium data of gas hydrates containing methane, propane, and hydrogen sulfide. *J. Chem. Eng. Data* 60:424–28
119. Davis JG, Rankin BM, Gierszal KP, Ben-Amotz D. 2013. On the cooperative formation of non-hydrogen bonded water at molecular hydrophobic interfaces. *Nat. Chem.* 5:796–802
120. Perera PN, Fega KR, Lawrence C, Sundstrom EJ, Tomlinson-Phillips J, Ben-Amotz D. 2009. Observation of water dangling OH bonds around dissolved nonpolar groups. *PNAS* 106:12230–34
121. Clark AH, Franks F, Pedley MD, Reid DS. 1977. Solute interactions in dilute-solutions. Part 2. Statistical mechanical study of hydrophobic interaction. *J. Chem. Soc. Faraday Trans. I* 73:290–305
122. Archer DG. 1989. Second virial-coefficients of aqueous alcohols at elevated-temperatures: a calorimetric study. *J. Phys. Chem.* 93:5272–79
123. Watanabe K, Andersen HC. 1986. Molecular dynamics study of the hydrophobic interaction in an aqueous solution of krypton. *J. Phys. Chem.* 90:795–802
124. Koga K, Widom B. 2013. Thermodynamic functions as correlation-function integrals. *J. Chem. Phys.* 138:114504
125. Raschke TM, Tsai J, Levitt M. 2001. Quantification of the hydrophobic interaction by simulations of the aggregation of small hydrophobic solutes in water. *PNAS* 98:5965–69
126. Rogers DM, Jiao D, Pratt LR, Remppe SB. 2012. Structural models and molecular thermodynamics of hydration of ions and small molecules. In *Annual Reports in Computational Chemistry*, ed. RR Wheeler, pp. 71–127. New York: Elsevier

127. Hands MD, Slipchenko LV. 2012. Intermolecular interactions in complex liquids: effective fragment potential investigation of water-*tert*-butanol mixtures. *J. Phys. Chem. B* 116:2775–86
128. Jencks WP. 1989. *Catalysis in Chemistry and Enzymology*. New York: McGraw Hill
129. Biedermann F, Nau WM, Schneider HJ. 2014. The hydrophobic effect revisited—studies with supramolecular complexes imply high-energy water as a noncovalent driving force. *Angew. Chem. Int. Ed.* 53:11158–71
130. Setny P, Baron R, McCammon JA. 2010. How can hydrophobic association be enthalpy driven? *J. Chem. Theory Comput.* 6:2866–71
131. Baron R, Setny P, McCammon JA. 2010. Water in cavity-ligand recognition. *J. Am. Chem. Soc.* 132:12091–97
132. Biedermann F, Uzunova VD, Scherman OA, Nau WM, De Simone A. 2012. Release of high-energy water as an essential driving force for the high-affinity binding of cucurbit[*n*]urils. *J. Am. Chem. Soc.* 134:15318–23
133. Ben-Amotz, D. 2016. Interfacial solvation thermodynamics. *J. Phys. Condens. Matter*. Submitted
134. Garde S, Patel AJ. 2011. Unraveling the hydrophobic effect, one molecule at a time. *PNAS* 108:16491–92
135. Cerdeirina CA, Debenedetti PG, Rossky PJ, Giovambattista N. 2011. Evaporation length scales of confined water and some common organic liquids. *J. Phys. Chem. Lett.* 2:1000–3
136. Li ITS, Walker GC. 2012. Single polymer studies of hydrophobic hydration. *Acc. Chem. Res.* 45:2011–21
137. Li ITS, Walker GC. 2011. Signature of hydrophobic hydration in a single polymer. *PNAS* 108:16527–32
138. Li ITS, Walker GC. 2012. Temperature, length scale and surface dependence of single polymer hydrophobic hydration. *Biophys. J.* 102(Suppl. 1):175a
139. Davis JG, Zukowski SR, Rankin BM, Ben-Amotz D. 2015. Influence of a neighboring charged group on hydrophobic hydration shell structure. *J. Phys. Chem. B* 8:9417–22
140. Pratt LR, Chandler D. 1980. Hydrophobic interactions and osmotic second virial-coefficients for methanol in water. *J. Solut. Chem.* 9:1–17
141. Asthagiri D, Merchant S, Pratt LR. 2008. Role of attractive methane-water interactions in the potential of mean force between methane molecules in water. *J. Chem. Phys.* 128:244512
142. Wanjari PP, Gibb BC, Ashbaugh HS. 2013. Simulation optimization of spherical non-polar guest recognition by deep-cavity cavitands. *J. Chem. Phys.* 139:234502
143. Shimizu S, Chan HS. 2000. Temperature dependence of hydrophobic interactions: a mean force perspective, effects of water density, and nonadditivity of thermodynamic signatures. *J. Chem. Phys.* 113:4683–700
144. Shimizu S, Chan HS. 2001. Anti-cooperativity in hydrophobic interactions: a simulation study of spatial dependence of three-body effects and beyond. *J. Chem. Phys.* 115:1414–21
145. Czaplewski C, Rodziewicz-Motowidlo S, Liwo A, Ripoll DR, Wawak RJ, Scheraga HA. 2000. Molecular simulation study of cooperativity in hydrophobic association. *Protein Sci.* 9:1235–45
146. Czaplewski C, Ripoll DR, Liwo A, Rodziewicz-Motowidlo S, Wawak RJ, Scheraga HA. 2002. Can cooperativity in hydrophobic association be reproduced correctly by implicit solvation models? *Int. J. Quantum Chem.* 88:41–55
147. Wang L, Friesner RA, Berne BJ. 2010. Hydrophobic interactions in model enclosures from small to large length scales: non-additivity in explicit and implicit solvent models. *Faraday Discuss.* 146:247–62
148. Matsumoto M. 2010. Four-body cooperativity in hydrophobic association of methane. *J. Phys. Chem. Lett.* 1:1552–56
149. Izvekov S. 2011. Towards an understanding of many-particle effects in hydrophobic association in methane solutions. *J. Chem. Phys.* 134:034104
150. Song B, Molinero V. 2013. Thermodynamic and structural signatures of water-driven methane-methane attraction in coarse-grained mW water. *J. Chem. Phys.* 139:054511